



**HAL**  
open science

**R<sub>8-x</sub> Ru<sub>3</sub> In<sub>7+x</sub> , R<sub>3</sub> Ru<sub>1-x</sub> In<sub>3</sub> , R<sub>39</sub> Ru<sub>12-x</sub> In<sub>35</sub> , and R<sub>16</sub> Ru<sub>5</sub> In<sub>14</sub> (R=La-Nd, Sm, Gd-Er, Lu) -  
New ternary indides with 2D intergrowth of CsCl- and  
AlB<sub>2</sub> -related slabs**

A. Tursina, V. Chernyshev, S. Nesterenko, H. Noël, M. Pasturel

► **To cite this version:**

A. Tursina, V. Chernyshev, S. Nesterenko, H. Noël, M. Pasturel. R<sub>8-x</sub> Ru<sub>3</sub> In<sub>7+x</sub> , R<sub>3</sub> Ru<sub>1-x</sub> In<sub>3</sub> , R<sub>39</sub> Ru<sub>12-x</sub> In<sub>35</sub> , and R<sub>16</sub> Ru<sub>5</sub> In<sub>14</sub> (R=La-Nd, Sm, Gd-Er, Lu) - New ternary indides with 2D intergrowth of CsCl- and AlB<sub>2</sub> -related slabs. *Journal of Alloys and Compounds*, 2019, 791, pp.641-647. 10.1016/j.jallcom.2019.03.224 . hal-02122176

**HAL Id: hal-02122176**

**<https://univ-rennes.hal.science/hal-02122176>**

Submitted on 13 May 2019

**HAL** is a multi-disciplinary open access archive for the deposit and dissemination of scientific research documents, whether they are published or not. The documents may come from teaching and research institutions in France or abroad, or from public or private research centers.

L'archive ouverte pluridisciplinaire **HAL**, est destinée au dépôt et à la diffusion de documents scientifiques de niveau recherche, publiés ou non, émanant des établissements d'enseignement et de recherche français ou étrangers, des laboratoires publics ou privés.

$R_{8-x}Ru_3In_{7+x}$ ,  $R_3Ru_{1-x}In_3$ ,  $R_{39}Ru_{12-x}In_{35}$ , and  $R_{16}Ru_5In_{14}$  (R=La-Nd, Sm, Gd-Er, Lu) - new ternary intermetallics with 2D intergrowth of CsCl- and AlB<sub>2</sub>-related slabs

Anna Tursina<sup>a</sup>, Vladimir Chernyshev<sup>a</sup>, Sergey Nesterenko<sup>a</sup>, Henri Noël<sup>b</sup>, Mathieu Pasturel<sup>b</sup>

<sup>a</sup> Department of Chemistry, Lomonosov Moscow State University, 119991, Moscow, Russia

<sup>b</sup> Univ Rennes, CNRS, Institut des Sciences Chimiques de Rennes – UMR6226, F-35042 Rennes, France

## Abstract

Twelve rare earth ruthenium intermetallics were synthesized by a two-step reaction and their crystal structures were determined by single-crystal X-ray diffraction.  $R_3Ru_{1-x}In_3$  (*Pbam*, *oP28*) and  $R_{16}Ru_5In_{14}$  (*P2/m*, *mP35*) crystallize with new structure types whereas  $R_{39}Ru_{12-x}In_{35}$  (*Pbam*, *oP172*) and  $R_{8-x}Ru_3In_{7+x}$  (*Pmma*, *oP36*) present occupation variants of  $Nd_{39}Ir_{10.98}In_{36.02}$  and  $Y_5Cu_5Mg_8$  structures, respectively. The new intermetallics are built of two different layers alternatively stacking along the shortest unit cell axis. The first layer is formed exclusively of rare-earth atoms while the second layer is built of ruthenium and indium thus displaying RIn and RRu fragments of CsCl type and RIn<sub>2</sub> and RRu<sub>2</sub> fragments of AlB<sub>2</sub> type.

Key-words: A. Intermetallics; A. Rare earth alloys and compounds; C. Crystal structure; D. X-ray diffraction

## Introduction

Some structures of rare-earth intermetallics (IMCs) with one short unit cell dimension ( $< 4 \text{ \AA}$ ) can be considered as 2D inhomogeneous intergrowths of CsCl- and AlB<sub>2</sub>-type slabs. Their general formula is given as  $R_{m+n}T_{2n}X_m$ , where R, T, and X accordingly are atoms of rare-earth, transition metal and *p*-element. The structures are composed of two different layers stacking along the shortest unit cell axis. The first layer is formed exclusively of rare-earth atoms while the second layer is built of transition metal and *p*-element thus displaying *m* RX fragments of CsCl-type and *n* RT<sub>2</sub> fragments of AlB<sub>2</sub>-type.

Some of the family members are widely encountered among the ternary intermetallics. The  $Lu_5Ni_2In_4$ -type structure ( $m=4$ ,  $n=1$ ) [1] is typical nearly for the whole row of rare earths with platinum as T element [2] and for the late rare earths with palladium [3]. The  $Nd_{11}Pd_4In_9$  structure type ( $m=9$ ,  $n=2$ ) [4] was found for nickel [5], cobalt [6], and palladium rare-earth intermetallics [7]. Numerous  $R_2T_2X$  IMCs crystallize with  $Mo_2FeB_2$  type structure ( $m=1$ ,  $n=1$ ) [8].

The first ruthenium intermetallic built of CsCl- and AlB<sub>2</sub>-type units -  $Ce_{11}Ru_{3.83}In_9$  [9] - was established to exist within the  $Nd_{11}Pd_4In_9$  type. Synthesis of other rare earth ruthenium intermetallics of the same composition yielded a variety of new compounds with new structure types [10]. To the

best of our knowledge, they are the first ruthenium indides based on rare earths other than Ce or La. Indeed, ternary rare earth ruthenium indides are still sparse compared to those with Pd and Pt. Besides  $\text{Ce}_{11}\text{Ru}_{3.83}\text{In}_9$ , they comprise eight compounds with cerium –  $\text{Ce}_{16}\text{Ru}_8\text{In}_{37}$  [11],  $\text{Ce}_{16}\text{Ru}_8\text{In}_3$  [12],  $\text{CeRu}_{0.88}\text{In}_2$  [13],  $\text{Ce}_3\text{Ru}_2\text{In}_2$  [14],  $\text{Ce}_2\text{Ru}_2\text{In}_3$  [14],  $\text{Ce}_{23}\text{Ru}_7\text{In}_4$  [15],  $\text{Ce}_4\text{RuIn}$  [16, 17] and  $\text{Ce}_3\text{Ru}_2\text{In}_3$  [18] – and two compounds with lanthanum –  $\text{La}_{21}\text{Ru}_{14}\text{In}_5$  [19] and  $\text{La}_9\text{Ru}_4\text{In}_5$  [20].

Herein we report on the synthesis and detailed structural characterization of the ruthenium indides -  $\text{R}_{11}\text{Ru}_4\text{In}_9$  (R=Gd, Tb),  $\text{R}_{8-x}\text{Ru}_3\text{In}_{7+x}$  (R=La, Pr, Nd, Sm, Gd, Tb, Dy),  $\text{R}_3\text{Ru}_{1-x}\text{In}_3$  (R=Tb, Ho, Er, Lu),  $\text{R}_{39}\text{Ru}_{12-x}\text{In}_{35}$  (R=Sm, Gd), and  $\text{R}_{16}\text{Ru}_5\text{In}_{14}$  (R= Dy, Ho, Er) built of the fragments of CsCl and  $\text{AlB}_2$  prototypes.

## Synthesis

Elemental components of high purity (rare earth ingots 99.85 wt%, Ru powder 99.99 wt%, and In ingots 99.999 wt%) were arc melted in an Edmund Bühler MAM-1 compact arc-furnace on a water-cooled copper hearth under an argon atmosphere with Zr getter. In order to minimize mass losses the ruthenium powder was initially arc-melted into buttons.

As the synthesis by direct reaction of the elements was not successful – a small amount of pure ruthenium was found in the crushed samples – a two stage synthesis was applied. Firstly, ruthenium and a rare-earth metal were arc-melted twice. In the second stage, indium was added to the binary alloy and arc melted at least three times to ensure homogeneity. Each of the arc-melting procedures included weighing of samples to control weight losses and addition of the appropriate amounts of a rare earth in order to maintain the initial stoichiometry. Subsequent annealing was performed at 873 K in evacuated quartz ampoules during one month. Reactions for all rare earths from La to Lu (except for Ce, Pm and Eu) were attempted. The desired ternary phases were not obtained for Tm and Yb.

Based on the stoichiometry of the first ruthenium indide -  $\text{Ce}_{11}\text{Ru}_4\text{In}_9$ , the initial composition of the alloys was 11R:4Ru:9In. As soon as the first structures were solved from single-crystal data a new series of synthesis based on the corrected stoichiometry was performed.

The compositions of the annealed polycrystalline samples and their microstructure were investigated by means of energy dispersive X-ray spectroscopy (EDX) using a Carl Zeiss LEO EVO 50XVP scanning electron microscope; equipped with an INCA Energy 450 (Oxford Instruments) EDX-spectrometer. The standard deviation of these measurements did not exceed 0.9 at.%.

Single crystals of nearly all the compounds were found on the surfaces of the as-cast samples with the exception of  $R_{8-x}Ru_3In_{7+x}$  IMCs. Single crystals of the latter compounds were extracted from the crushed samples after annealing procedure.

### Single-crystal XRD

Single crystal data for  $Lu_3Ru_{0.97}In_3$ ,  $Tb_{7.60}Ru_3In_{7.40}$ ,  $Pr_8Ru_3In_7$ ,  $Gd_{39}Ru_{11.63}In_{35}$ ,  $Sm_{39}Ru_{11.68}In_{35}$ ,  $Sm_{7.72}Ru_3In_{7.28}$ , and  $Ho_{16}Ru_5In_{14}$  were collected at room temperature on a Bruker Apex II diffractometer (MoK $\alpha$  radiation). An empirical absorption correction was applied using the program SADABS [21]. Single-crystal intensity data for  $Tb_3Ru_{0.97}In_3$ ,  $Ho_3Ru_{0.96}In_3$ ,  $Er_3Ru_{0.91}In_3$ ,  $Dy_{16}Ru_5In_{14}$ , and  $Gd_8Ru_3In_7$  were collected by using a CAD4 Enraf Nonius diffractometer (AgK $\alpha$  radiation). An empirical absorption correction was done on the basis of  $\Psi$ -scan data [22]. The relevant crystallographic details of the data collections and the structure refinements are listed in Table 1.

The crystal structures were solved by direct methods using SHELXS-97 [23] and refined using SHELXL-97 [23] (full-matrix least-squares on  $F^2$ ) with anisotropic displacement parameters for all atoms in the unit cells. The data on the single crystal structures of IMCs were deposited at the Inorganic Crystal Structure Database (ICSD, Karlsruhe) and may be obtained from the Fachinformationszentrum Karlsruhe, 76344 Eggenstein-Leopoldshafen, Germany (Fax: +49-7247-808-666; E-Mail: [crysdata@fiz-karlsruhe.de](mailto:crysdata@fiz-karlsruhe.de), [http://www.fiz-karlsruhe.de/request\\_for\\_deposited\\_data.html](http://www.fiz-karlsruhe.de/request_for_deposited_data.html)) on quoting the following depository numbers: CSD 434543 ( $Tb_{7.60}Ru_3In_{7.40}$ ), CSD 434533 ( $Pr_8Ru_3In_7$ ), CSD 434221 ( $Gd_{39}Ru_{11.63}In_{35}$ ), CSD 434222 ( $Sm_{39}Ru_{11.68}In_{35}$ ), CSD 434075 ( $Ho_{16}Ru_5In_{14}$ ), CSD 433893 ( $Tb_3Ru_{0.97}In_3$ ), CSD 433894 ( $Ho_3Ru_{0.96}In_3$ ), CSD 434069 ( $Dy_{16}Ru_5In_{14}$ ), CSD 434551 ( $Sm_{7.72}Ru_3In_{7.28}$ ), and CSD 433888 ( $Gd_8Ru_3In_7$ ). Further details on the crystal structure refinement of  $Lu_3Ru_{0.97}In_3$  and  $Er_3Ru_{0.91}In_3$  can be obtained complimentary from the joint CCDC/FIZ Karlsruhe database via [www.ccdc.cam.ac.uk/data\\_request/cif](http://www.ccdc.cam.ac.uk/data_request/cif) by quoting the reference number CCDC1874079 and CCDC1898839, respectively.

### Powder XRD

Polycrystalline samples of the new IMCs which were expected to be nearly single-phase from EDX analysis were studied by powder XRD. Measurements were performed at the ESRF (Grenoble, France) at the high-resolution powder diffraction beamline ID22 equipped with a cryogenically cooled double-crystal Si(111) monochromator and a Si(111) analyzer [24]. Thin-walled glass capillaries (0.5 mm diameter) containing IMC powders were rotated during measurements at a rate of 1200 rpm to improve the counting statistics. The calibration of the



$R_{11}Ru_4In_9$		[8]				p	p				
$R_3Ru_{1-x}In_3$							s		s	s	s
$R_{16}Ru_5In_{14}$								s, p	s	p	
$R_{39}Ru_{12-x}In_{35}$					s	s					
$R_{8-x}Ru_3In_{7+x}$	p		s	p	s, p	s, p	s, p				

\*p = powder data, s = single crystal data

$R_3Ru_{1-x}In_3$  and  $R_{16}Ru_5In_{14}$  compounds form with new types of IMCs, and  $R_{39}Ru_{12-x}In_{35}$  and  $R_{8-x}Ru_3In_{7+x}$  are occupation variants of  $Nd_{39}Ir_{10.98}In_{36.02}$  [26] and  $Y_5Cu_5Mg_8$  [27] structures, respectively. The  $Nd_{11}Pd_4In_9$  structure type [4] was described in detail in [4-7], so we will not analyze the isostructural  $Gd_{11}Ru_4In_9$  and  $Tb_{11}Ru_4In_9$  IMCs in the present work.

### $R_3Ru_{1-x}In_3$ (R=Tb, Ho, Er, Lu) crystal structures

$Tb_3Ru_{0.97}In_3$ ,  $Ho_3Ru_{0.96}In_3$ ,  $Er_3Ru_{0.91}In_3$ , and  $Lu_3Ru_{0.98}In_3$  crystallize with a new structure type. Its orthorhombic unit cell (space-group Pbam, no. 55) consists of seven crystallographic sites, each occupied by a unique atom sort (Supplementary Table S1). All the atoms display  $..m$  site symmetry with  $z=1/2$  for rare earth positions and  $z=0$  for ruthenium and indium atoms positions. In contrast to the fully occupied rare-earth and indium crystallographic sites, the occupancy of that of ruthenium is lower than 100% which was earlier observed for ruthenium atom in rare-earth ruthenium indides  $Ce_{11}Ru_{3.83}In_9$  [9] and  $CeRu_{0.88}In_2$  [13].

Two types of rare-earth coordination polyhedra are observed in this structure type (Fig. 2a). The R1 atom is enclosed in a  $[Ru_2In_6]$  tetragonal prism capped on all faces by R-atoms to form  $R1[R_6Ru_2In_6]$  coordination polyhedra. R2 and R3 atoms are surrounded by 15 and 14 neighbors in the form of pentagonal prisms capped on both basal faces and on three and two side faces, respectively –  $R2[R_5Ru_2In_8]$  and  $R3[R_4Ru_2In_8]$ . Ruthenium atom is coordinated by a triangular prism of six R atoms with three indium atoms capping the side faces of the  $Ru[R_6In_3]$  prism. Three crystallographically inequivalent indium sites have different coordination environments and coordination numbers. In1 is located inside a triangular prism capped on all faces -  $In1[R_6In_5]$ . Coordination polyhedra of In2 and In3 atoms can be presented as distorted tetragonal prisms centered on four and five faces, respectively –  $In2[R_8RuIn_3]$  and  $In3[R_8Ru_2In_3]$ .

The shortest interatomic distances R-In and In-In are below the sums of respective atomic radii. R-Ru contacts are significantly smaller than the sum of R and Ru metallic radii of  $\sim 3.1 \text{ \AA}$  (Supplementary Table S2). Ru-In interactions exceed the sum of metallic radii. R-R contacts, in turn, are approximately equal to or larger than the double metallic radii of the elements.

### $R_{16}Ru_5In_{14}$ (R=Dy - Er) crystal structures

$R_{16}Ru_5In_{14}$  compounds crystallize in a novel structure type. This structure type seems to be relatively complex as it contains 17 independent Wyckoff positions in space group  $P2/m$  (Supplementary Table S3). All crystallographic positions are fully occupied by a unique atom kind. The Ru1 atom occupies the  $1a$  position with  $2/m$  symmetry while all other sites display  $m$  symmetry with R atoms at  $y=1/2$  and In and Ru atoms at  $y=0$ .

Coordination polyhedra of rare-earth atoms can be presented as distorted tetragonal (R1-R3, R5, R8) and pentagonal (R4, R6, R7) prisms centered on the basal faces and on some of the side faces (Fig. 2b). Within the coordination polyhedra, R-In contacts are slightly smaller or approximately equal to the sum of the R and In radii (Supplementary Table S4). In contrast, all the R-Ru interatomic distances are noticeably smaller than the sum of the element radii, in agreement with the observations on the previous structure-type. The coordination environment of Ru1 and Ru2 atoms consists of six rare-earth atoms and three indium atoms which form slightly distorted tricapped triangular prisms with interatomic distances in the range of 2.775-3.177 Å and 2.781-3.161 Å for Dy and Ho compounds, respectively. The Ru3 atom is surrounded by eight rare earths in the form of practically ideal cube and a narrow range of R-Ru contacts – 2.980-3.040 Å. The In6 atom is located in a distorted triangular prism of six rare-earth atoms capped on all side faces by two indium atoms and one ruthenium atom with the shortest Ru2-In6 contact of 2.78 Å. The other six indium atoms reside in equatorially capped distorted tetragonal prisms, In-In contacts all being shorter the double metallic radius of In.

### **$R_{39}Ru_{12-x}In_{35}$ (R=Sm, Gd) crystal structures**

The structures of  $Sm_{39}Ru_{11.68}In_{35}$  and  $Gd_{39}Ru_{11.63}In_{35}$  represent a partial occupancy variant of the  $Nd_{39}Ir_{10.98}In_{36.02}$  type [26]. A complex intergrowth structure built of CsCl- and  $AlB_2$ -related slabs constituted of 44 atomic positions (Fig. 3 and Supplementary Table S5). In spite of a rather complex composition the structures are perfectly ordered and coordination polyhedra of atoms can be easily described in terms of centered triangular, tetragonal and pentagonal prisms. Thus, rare-earth atoms reside in either tetragonal or pentagonal prisms built of Ru and In-atoms (Supplementary Table S6). Slightly distorted triangular  $[R_6]$  prisms equatorially tri-capped by indium atoms are typical for all ruthenium atoms. Two of the 18 indium sites have a triangular prismatic environment while the other 16 indium atoms are located inside tetragonal prisms.  $R_{39}Ru_{12-x}In_{35}$  structures differ from the  $Nd_{39}Ir_{10.98}In_{36.02}$  prototype by the following. If in  $Nd_{39}Ir_{10.98}In_{36.02}$  Ir and In statistically occupy one of the  $4g$  sites, in  $R_{39}Ru_{12-x}In_{35}$  the corresponding site is occupied by Ru. Another feature of  $R_{39}Ru_{12-x}In_{35}$  structures is a partial occupancy (~90%) of both Ru5 and Ru6 positions.

**$R_{8-x}Ru_3In_{7+x}$  (R=La, Pr, Nd, Sm, Gd, Tb) crystal structures**

$R_{8-x}Ru_3In_{7+x}$  (R= La, Pr, Nd, Sm, Gd, Tb) crystallize with an occupancy version of the  $Y_5Cu_5Mg_8$  structure [27]. In contrast to the above described structures discovered exclusively for the representatives of the late rare earths, this type was found nearly for all rare earths including the early ones. Going from  $La_8Ru_3In_7$  to  $Tb_8Ru_3In_7$ , a significant shortening of the cell parameters is observed which agrees well with the lanthanide contraction (Table 2).

A structural peculiarity of this type of IMC is a split R5 position, of about 0.4 Å in the *c*-direction, for some of the representatives (Sm, Tb) (Fig. 3). Special cycles of least-squares refinement were aimed to estimate the atom sorts occupying the split position. Analysis of the refinement results and interatomic distances around the split positions unambiguously indicates that rare earths (R5) and indium (In5) are separately located over the split position (Supplementary Table S7). As a consequence, rare-earth and indium content tends to converge, which was definitely confirmed by EDX analyses of the appropriate phases.

The closely structurally related compounds -  $Y_5Cu_5Mg_8$  [27] and  $R_{8-x}Ru_3In_{7+x}$  – exhibit a different distribution of the element types over the crystallographic sites. In  $Y_5Cu_5Mg_8$  coordination arrangement around each element is clearly distinguished: Y atoms are situated in pentagonal prisms, Mg atoms are distributed in tetragonal prisms, and Cu atoms - in trigonal prisms. It results in a stacking along the *b*-axis of two different layers, the composition of the first one ( $y=1/2$ ) being  $[Y_{10}Cu_2Mg_4]$  and composition of the second one  $[Cu_8Mg_{12}]$ . Compared to  $Y_5Cu_5Mg_8$ , in the  $R_{8-x}Ru_3In_{7+x}$  structure the atoms are not so orderly coordinated. Breaking the order, R1 and R5(/In5) atoms are enclosed by tetragonal prisms (respective Mg2 and Mg5 sites in  $Y_5Cu_5Mg_8$ ) and In2 atoms by trigonal prisms (respective Cu2 site), accordingly. Thus, in  $R_{8-x}Ru_3In_{7+x}$  structure the compositions of the two layers are  $[R_{12}Ru_2]$  ( $y=1/2$ ) and  $[R_2Ru_4In_{14}]$  ( $y=0$ ) which does not correspond to the ideal architecture of layers observed for the compounds of the  $R_{m+n}T_{2n}X_m$  family. Consequently, if this new structure-type can be mainly described as a stacking of CsCl- and AlB<sub>2</sub>-units, different kinds of bricks also have to be used in the vicinity of the R5(/In5) atoms.

**Crystal chemical peculiarities of the new structures**

The structures of  $Lu_5Ni_2In_4$  [1],  $Nd_{11}Pd_4In_9$  [3],  $Nd_4Co_2Mg_3$  [28], *o*- $La_2Ni_2In$  [29] form a homologous series based on a 2D intergrowth of AlB<sub>2</sub>- and CsCl-type slabs described by the general formula  $R_{m+n}T_{2n}X_m$  (R, T, and X accordingly are atoms of rare-earth, transitional metal and p-element) (Fig. 4). Likewise, atomic arrangement in some transition metal borides such as

$\text{Mo}_2\text{FeB}_2$  [8],  $\text{Nb}_7\text{Fe}_3\text{B}_8$  [30],  $\text{Ru}_9\text{Al}_5\text{B}_{8-x}$  [31, 32],  $\text{Fe}_3\text{Al}_2\text{B}_2$  [31], and  $\text{Ru}_4\text{Al}_3\text{B}_2$  [32] can be described as  $\text{T}_{m+n}\text{T}'_m\text{B}_{2n}$  family members built of a 2D intergrowth of  $\text{TB}_2$  fragments of  $\text{AlB}_2$ -type and  $\text{TT}'$  fragments of CsCl-type (Fig. 4).

All four new types of structure presented in this article are fully or mainly built of CsCl and  $\text{AlB}_2$  fragments. However, none of them follows the general formula  $\text{R}_{m+n}\text{T}_{2n}\text{X}_m$ .

The structures are built from two types of layers running perpendicular to the short axis (Fig. 3). The first layer is formed solely of rare-earth atoms whereas the second layer consists of ruthenium and indium atoms. The only exception is the  $\text{R}_{8-x}\text{Ru}_3\text{In}_{7+x}$  structure where one of the ruthenium atoms (Ru2) breaks the ideal arrangement and resides inside the “rare-earth layer” and one of the rare-earth atoms (R5) resides in the Ru-In slab. Keeping in mind this distortion let us define the main peculiarities of the new structures. If the structures described by the formula  $\text{R}_{m+n}\text{T}_{2n}\text{X}_m$  are composed of  $m$  RX fragments of CsCl-type and  $n$   $\text{RT}_2$  fragments of  $\text{AlB}_2$ -type, the new structures reveal two new types of fragments – RT fragments of CsCl-type and  $\text{RX}_2$  fragments of  $\text{AlB}_2$ -type. Thus, in the  $\text{R}_{8-x}\text{Ru}_3\text{In}_{7+x}$ ,  $\text{R}_3\text{Ru}_{1-x}\text{In}_3$ , and  $\text{Sm}_{39}\text{Ru}_{12-x}\text{In}_{35}$  structures, we observe  $\text{RIn}_2$  fragment of  $\text{AlB}_2$ -type along with  $\text{RIn}$  fragments of CsCl-type and  $\text{RRu}_2$  fragments of  $\text{AlB}_2$ -type. The structure of  $\text{R}_{16}\text{Ru}_5\text{In}_{14}$  comprises four types of fragments -  $\text{RIn}$  and  $\text{RRu}$  fragments of CsCl-type and  $\text{RRu}_2$  and  $\text{RIn}_2$  fragments of  $\text{AlB}_2$ -type. Fig. 2 presents a view of the new structures projected along the short axis. Because of In radius being 0.25 Å larger than that of Ru, R-In contacts are longer than those of R-Ru by 0.15 Å and more. This is distinctly visible in Fig. 2 wherein the area of a basal face of trigonal prism centered by In is greater than those centered by Ru. The same is peculiar for the rectangular prisms centered by In or Ru atoms – the area of a basal face is greater for the In-centered prisms (see  $\text{R}_{16}\text{Ru}_5\text{In}_{14}$  structure).

## Conclusion

New compounds extend the family of ternary rare earth ruthenium intermetallics which was previously restricted to the representatives of cerium and lanthanum. All four new types of structure -  $\text{R}_3\text{Ru}_{1-x}\text{In}_3$ ,  $\text{R}_{16}\text{Ru}_5\text{In}_{14}$ ,  $\text{R}_{39}\text{Ru}_{12-x}\text{In}_{35}$ , and  $\text{R}_{8-x}\text{Ru}_3\text{In}_{7+x}$  - can be presented as built of the  $\text{RIn}$  and  $\text{RRu}$  fragments of CsCl type and  $\text{RIn}_2$  and  $\text{RRu}_2$  of  $\text{AlB}_2$  type displaying more complex variants of a 2D inhomogeneous intergrowth compared to IMCs with general formula of  $\text{R}_{m+n}\text{T}_{2n}\text{X}_m$ .

## Acknowledgements

The authors thank ESRF for providing an access to ID22 beamline, experiment MA-3313. This research was supported by RFBR (research Grant No. 19-03-00135).

**Figure captions.**

1. Rietveld refined PXRD pattern of a  $\text{Dy}_{16}\text{Ru}_5\text{In}_{14}$  sample showing the experimental (black) and difference (red) profiles ( $\chi^2 = 7.511$ ,  $R_p = 0.042$ ,  $R_{wp} = 0.060$ ,  $R_{exp} = 0.020$ ). The blue vertical bars denote the calculated positions of the Bragg peaks.
2. (a) Unit cell projection of the  $\text{R}_3\text{Ru}_{1-x}\text{In}_3$  structure onto the  $(a,b)$  plane. The network of four- and five-membered rings at  $z=0$  is shown by solid lines, the networks of three- and four-membered rings at  $z=1/2$  is shown by dotted lines. (b) Unit cell projection of the  $\text{R}_{16}\text{Ru}_5\text{In}_{14}$  structure onto the  $(a,c)$  plane. The network of four- and five-membered rings at  $y=0$  is shown by solid lines, the network of three- and four-membered rings at  $y=1/2$  is shown by dotted lines. R atoms are drawn as big green balls, Ru atoms as blue balls, and In atoms as pink balls.
3. Projections of the  $\text{R}_3\text{Ru}_{1-x}\text{In}_3$ ,  $\text{R}_{16}\text{Ru}_5\text{In}_{14}$ ,  $\text{R}_{39}\text{Ru}_{12-x}\text{In}_{35}$ , and  $\text{R}_{8-x}\text{Ru}_3\text{In}_{7+x}$  structures along the short unit cell axis presented as members of inhomogeneous 2D intergrowth structure series with  $\text{AlB}_2$ - and  $\text{CsCl}$ -type constructive units.
4. Projections along the short unit cell axis of the crystal structures of  $\text{R}_{m+n}\text{T}_{2n}\text{X}_m$  and  $\text{T}_{m+n}\text{T}'_m\text{B}_{2n}$  homologous series as a combination of  $\text{AlB}_2$ - and  $\text{CsCl}$ -type fragments.

## References

1. V.I. Zaremba, Ya.M. Kalychak, P.Yu. Zavalii, V.A. Bruskov, Crystal structure of the compounds  $R_5Ni_2In_4$  (R=Ho, Er, Tm, Lu), *Krystallografiya*, 36 (1991) 1415-1418.
2. R. Zaremba, U. Ch. Rodewald, and R. Pöttgen, Rare Earth-Rich Indides  $RE_5Pt_2In_4$  (RE=Sc, Y, La–Nd, Sm, Gd–Tm, Lu), *Monatsh. Chem.*, 138 (2007) 819–822.  
<http://dx.doi.org/10.1007/s00706-007-0702-6>.
3. L.D. Sojka, M. Dashkevych, B.D. Belan, M.D. Manyako, V.M. Davydov, L.G. Akselrud, Ya.M. Kalychak, Crystal structure of alloys  $R_5Pd_2In_4$  (R = Y, Tb, Dy, Ho, Er, Tm, Lu), *Ukr. Chem. J.*, 74 (2008) 90-94.
4. L. Sojka, M. Manyako, R. Cerny, M. Ivanyk, B. Belan, R. Gladyshevskii, Ya. Kalychak,  $Nd_{11}Pd_4In_9$  compound - A new member of the homological series based on  $AlB_2$  and  $CsCl$  types, *Intermetallics*, 16 (2008) 625-628. <https://doi.org/10.1016/j.intermet.2008.01.001>.
5. M. Pustovoychenko, Yu. Tyvanchuk, I. Hayduk, Ya. Kalychak, Crystal structure of the  $RE_{11}Ni_4In_9$  compounds (RE = La, Ce, Pr, Nd, Sm, Gd, Tb and Y), *Intermetallics*, 18 (2010) 929–932. <https://doi.org/10.1016/j.intermet.2010.01.003>.
6. Yu. Tyvanchuk, M. Dzevenko, Ya. Kalychak,  $R_{11}Co_4In_9$  (R = Gd, Tb, Dy, Ho, Er) – The first representatives of  $Nd_{11}Pd_4In_9$  structure type in R–Co–In systems, *Visn. L'viv Univ. Ser. Khim.*, 53 (2012) 127-132.
7. L. Sojka, M. Demchyna, B. Belan, M. Manyako, Ya. Kalychak, New compounds with  $Nd_{11}Pd_4In_9$  structure type in the systems RE-Pd-In (RE = La, Ce, Pr, Nd, Sm, Gd, Tb, Dy) *Intermetallics*, 49 (2014) 14-17. <https://doi.org/10.1016/j.intermet.2014.01.003>.
8. W. Rieger, H. Nowotny, F. Benesovsky, Die Kristallstruktur von  $Mo_2FeB_2$ . *Monatsh. Chem.*, 95 (1964) 1502-1503. <https://doi.org/10.1007/BF00901704>.
9. V. Gribova, E. Murashova, D. Gnida, Zh. Kurenbaeva, S. Nesterenko, A. Tursina, D. Kaczorowski, A. Gribov, Novel ternary cerium-rich intermetallic compound  $Ce_{11}Ru_{3.83}In_9$ : Crystal structure and low-temperature physical properties, *J. Alloys Compd.*, 711 (2017) 455-461. <https://doi.org/10.1016/j.jallcom.2017.03.168>.
10. A. Tursina, S. Nesterenko, T. Roisnel, H. Noël, New ternary indides with 2D intergrowth  $CsCl$ - and  $AlB_2$ -related slabs, The 21st International Conference on Solid Compounds of Transition Elements, March 25 - 29, 2018, Program and Abstracts, p.20.
11. E.V. Murashova, Zh.M. Kurenbaeva, A.I. Tursina, H. Noël, P. Rogl, A.V. Grytsiv, A.V. Gribov, G. Giester, Yu.D. Seropegin, The crystal structure of  $Ce_{16}Ru_8In_{37}$ , *J. Alloy. Compd.*, 442 (2007) 89-92. <https://doi.org/10.1016/j.jallcom.2006.08.346>.
12. Zh.M. Kurenbaeva, A.I. Tursina, E.V. Murashova, S.N. Nesterenko, Yu.D. Seropegin, Synthesis and crystal structure of a new ternary intermetallic compound  $Ce_{16}Ru_{8-x}In_{3-x}$  ( $0 <$

$x < 1.0$ ), Russ. J. Inorg. Chem., 56 (2011) 218-222.

<https://doi.org/10.1134/S003602361102015X>.

13. E.V. Murashova, A.I. Tursina, Zh.M. Kurenbaeva, A.V. Griбанov, Yu.D. Seropegin, Crystal structure of  $CeRu_{0.88}In_2$ , J. Alloy. Compd., 454 (2008) 206-209.  
<https://doi.org/10.1016/j.jallcom.2006.12.123>.
14. A.I. Tursina, Zh.M. Kurenbaeva, A.V. Griбанov, H. Noel, Yu.D. Seropegin,  $Ce_2Ru_2In_3$  and  $Ce_3Ru_2In_2$ : site exchange in ternary indides of a new structure type, J. Alloy. Compd., 442 (2007) 100-103. <https://doi.org/10.1016/j.jallcom.2006.09.146>.
15. Zh.M. Kurenbaeva, E.V. Murashova, S.N. Nesterenko, A.I. Tursina, V.A. Griбанова, Yu.D. Seropegin, H. Noël, Novel ternary intermetallics from Ce-Ru-In system with high content of cerium, in: Collected Abstracts of XXII International Conference on Crystal Chemistry of Intermetallic Compounds, Lviv, Ukraine, September 22-26, 2013, p. 105.
16. Zh.M. Kurenbaeva, E.V. Murashova, D.N. Hannanov, A.B. Ilyukin, A.I. Tursina, Y.D. Seropegin, Ternary intermetallics  $La_4RuAl$ ,  $Ce_4RuAl$ , and  $Ce_4RuIn$ , in: Collected Abstracts of XI International Conference on Crystal Chemistry of Intermetallic Compounds. Lviv, Ukraine, May 30 – June 2, 2010, p. 103.
17. F. Tappe, C. Schwickert, S. Linsinger, R. Pöttgen, New rare earth-rich aluminides and indides with cubic  $Gd_4RhIn$ -type structure, Monatsh. Chem., 142 (2011) 1087–1095.  
<https://doi.org/10.1007/s00706-011-0622-3>.
18. Zh.M. Kurenbaeva, A.I. Tursina, E.V. Murashova, S.N. Nesterenko, A.V. Griбанov, Yu.D. Seropegin, H. Noël, Crystal structure of the new ternary compound  $Ce_3Ru_2In_3$ , J. Alloy. Compd., 442 (2007) 86-88. <https://doi.org/10.1016/j.jallcom.2006.09.145>.
19. A.I. Tursina, S.G. Cherviakov, H. Noël, V.V. Chernyshev, Y.D. Seropegin, Lanthanum ruthenium indide,  $La_{21}Ru_{9+x}In_{5-x}$  ( $x = 1.2$ ), Acta Cryst., E66 (2010) i40. inorganic compounds. <https://doi.org/10.1107/S1600536810014509>.
20. K. Shablinskaya, E. Murashova, A. Tursina, Zh. Kurenbaeva, A. Yaroslavtsev, Y. Seropegin, Intermetallics  $La_9Ru_4In_5$  and  $Ce_9Ru_4Ga_5$  with new types of structures. Synthesis, crystal structures, physical properties, Intermetallics, 23 (2012) 106-110.  
<https://doi.org/10.1016/j.intermet.2011.12.024>.
21. G.M. Sheldrick, SADABS, Program for Empirical Absorption Correction for Area Detector Data, University of Gottingen, Gottingen, Germany, 1996.
22. L.J. Farrugia, WinGX suite for small-molecule single-crystal crystallography, J. Appl. Cryst., 32 (1999) 837–838. <https://doi.org/10.1107/S0021889899006020>.
23. G.M. Sheldrick, A short history of SHELX, Acta Cryst. A 64 (2008) 112–122.  
<https://doi.org/10.1107/S0108767307043930>.

24. A.N. Fitch, The High Resolution Powder Diffraction Beam Line at ESRF, *J. Res. National Institute of Standards and Technology*, 109 (2004) 133–142.  
<http://dx.doi.org/10.6028/jres.109.010>.
25. V.B. Zlokazov, V.V. Chernyshev, MRIA - a program for a full profile analysis of powder multiphase neutron-diffraction time-of-flight (direct and Fourier) spectra, *J. Appl. Cryst.*, 25 (1992) 447-451. computer programs. <https://doi.org/10.1107/S0021889891013122>.
26. N. Dominyuk, V.I. Zaremba, U.Ch. Rodewald, R. Pöttgen,  $\text{Nd}_{39}\text{Ir}_{10.98}\text{In}_{36.02}$  – A complex intergrowth structure with CsCl- and  $\text{AlB}_2$  -related slabs, *Z. Naturforsch.*, 70b (2015) 497-503. <https://doi.org/10.1515/znb-2015-0054>.
27. P. Solokha, S. De Negri, V. Pavlyuk, A. Saccone, Inhomogeneous 2D linear intergrowth structures among novel Y–Cu–Mg ternary compounds with yttrium/copper equiatomic ratio, *Solid State Sci.*, 11 (2009) 801–811.  
<https://doi.org/10.1016/j.solidstatesciences.2008.12.006>.
28. S. Tuncel, R.-D. Hoffmann, B. Heying, B. Chevalier, R. Pöttgen, New Intermetallic Compounds  $\text{Nd}_4\text{Co}_2\text{Mg}_3$  and  $\text{Sm}_4\text{Co}_2\text{Mg}_3$  - an Intergrowth of  $\text{AlB}_2$  and CsCl Related Slabs, *Z. Anorg. Allg. Chem.*, 2006 (632) 2017-2020. <https://doi.org/10.1002/zaac.200600113>.
29. M. Pustovoychenko, V. Svitlyk, Ya. Kalychak, Orthorombic  $\text{La}_2\text{Ni}_2\text{In}$  form - A new intergrowth CsCl - and  $\text{AlB}_2$  - type slabs, *Intermetallics*, 24 (2012) 30-32.  
<https://doi.org/10.1016/j.intermet.2012.01.007>.
30. Q. Zheng, R. Gumeniuk, H. Borrmann, W. Schnelle, A.A. Tsirlin, H. Rosner, U. Burkhardt, M. Reissner, Y. Grin, A. Leithe-Jasper, Ternary borides  $\text{Nb}_7\text{Fe}_3\text{B}_8$  and  $\text{Ta}_7\text{Fe}_3\text{B}_8$  with Kagome-type iron framework, *Dalton Trans.*, 45 (2016) 9590-9600.  
<https://doi.org/10.1039/c6dt01164k>.
31. S. Hirt, F. Hilfinger, H. Hillebrecht, Synthesis and crystal structures of the new ternary borides  $\text{Fe}_3\text{Al}_2\text{B}_2$  and  $\text{Ru}_9\text{Al}_3\text{B}_8$  and the confirmation of  $\text{Ru}_4\text{Al}_3\text{B}_2$  and  $\text{Ru}_9\text{Al}_5\text{B}_{8-x}$  ( $x \approx 2$ )  
*Z. Kristall. Cryst. Mater.*, 233 (2018) 295-307. <https://doi.org/10.1515/zkri-2017-2095>.
32. W. Jung, K. Schweitzer, Die Kristallstrukturen der ternären Boride  $\text{Al}_2\text{Ru}_3\text{B}_2$  und  $\text{Al}_3\text{Ru}_4\text{B}_2$ , *Z. Kristall.* 178 (1988) 109–110. <https://doi.org/10.1524/zkri.1986.174.14.1>.

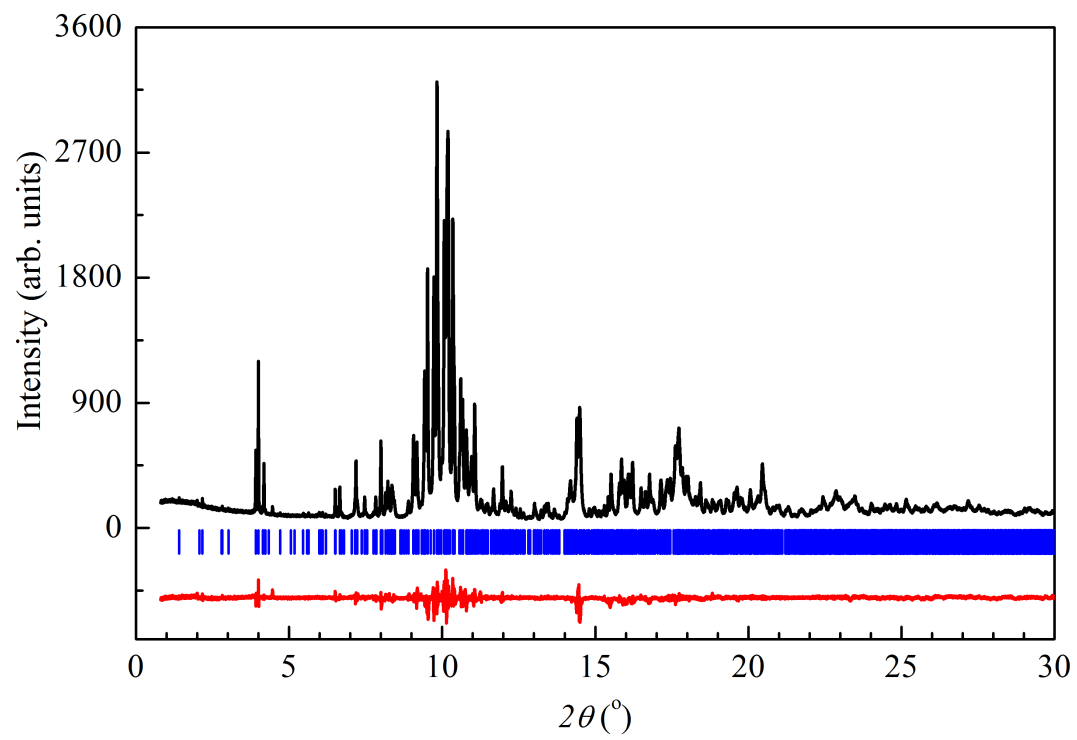
Table 1

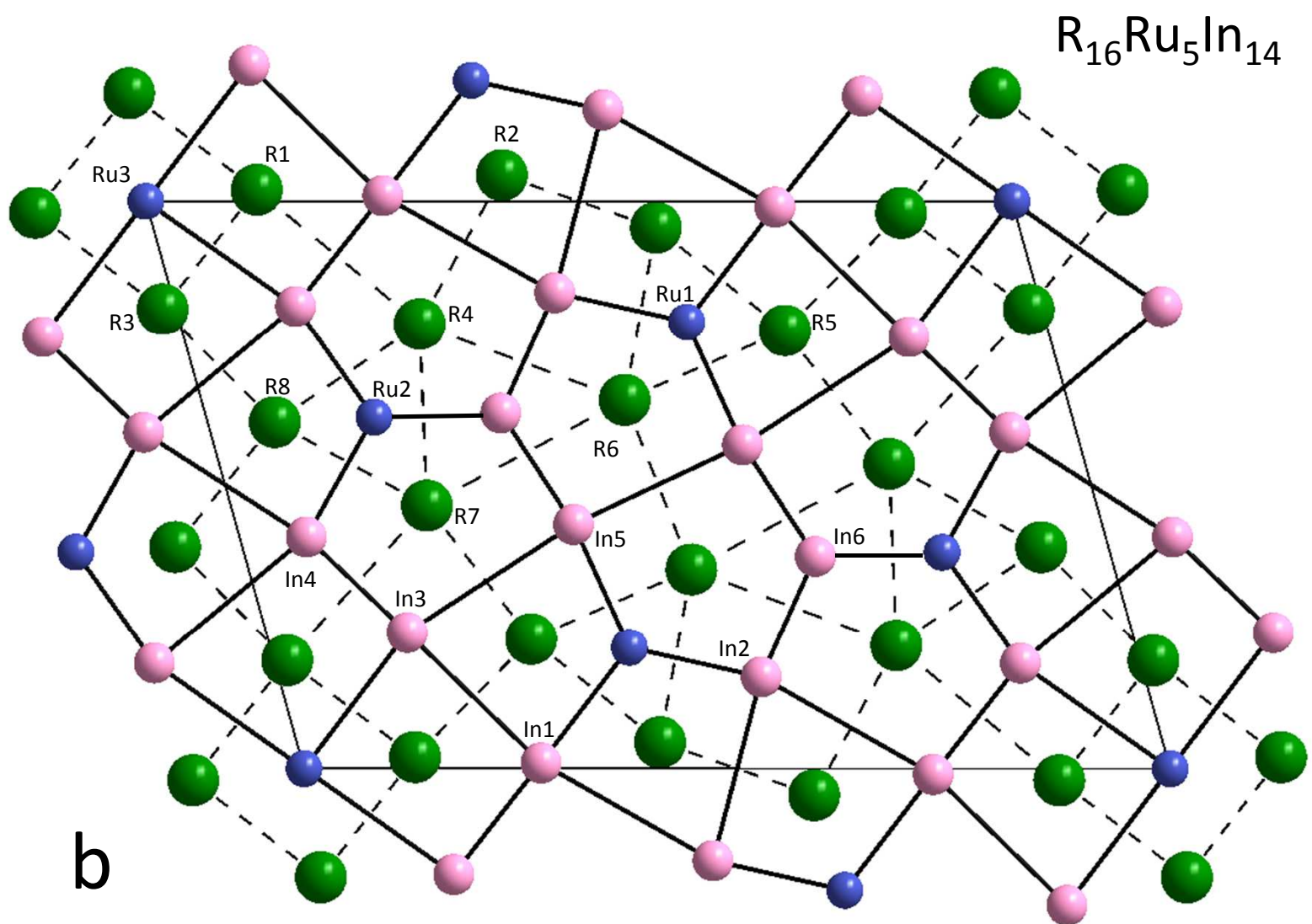
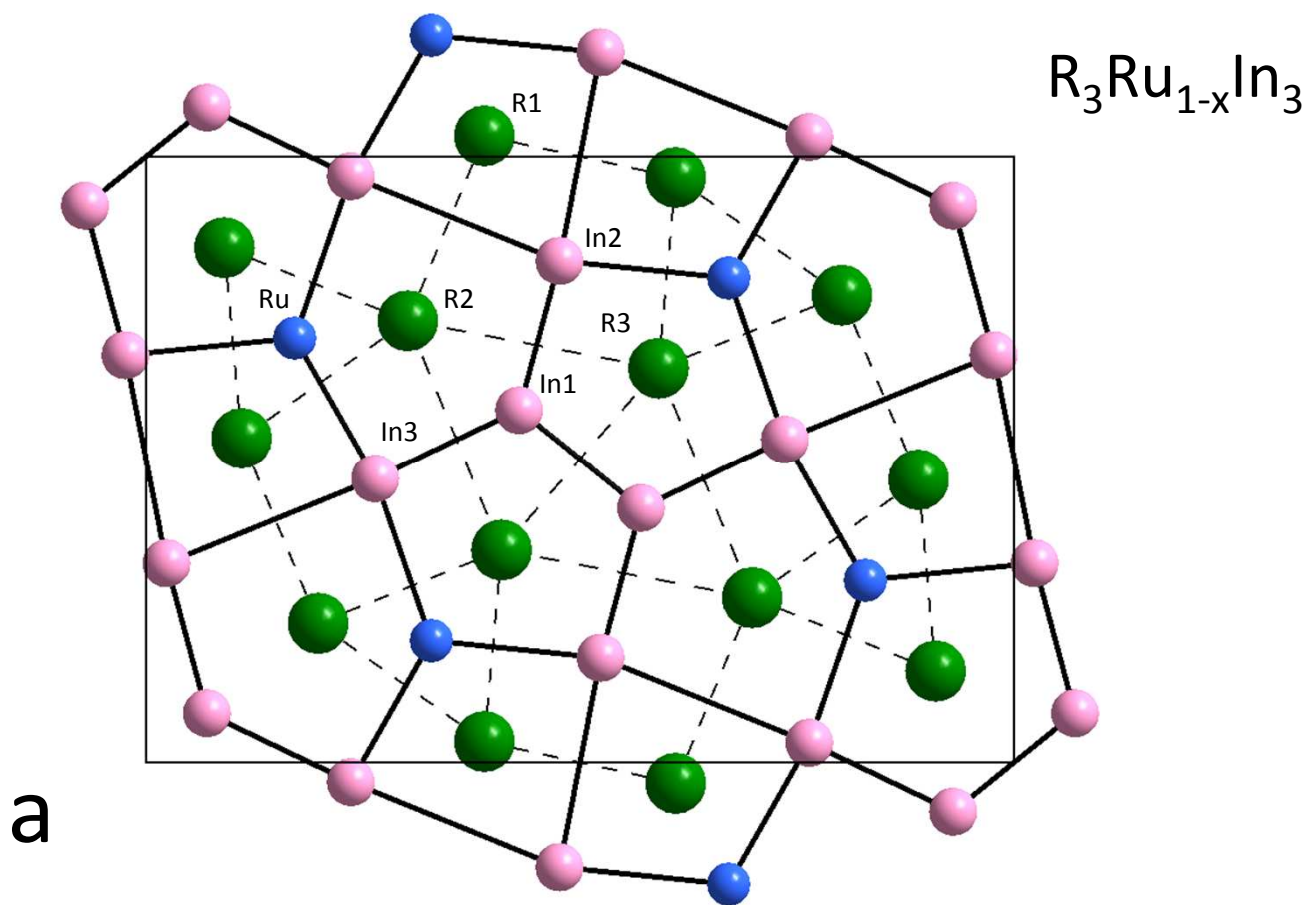
Crystallographic data and details of single crystals structure refinement for the new compounds

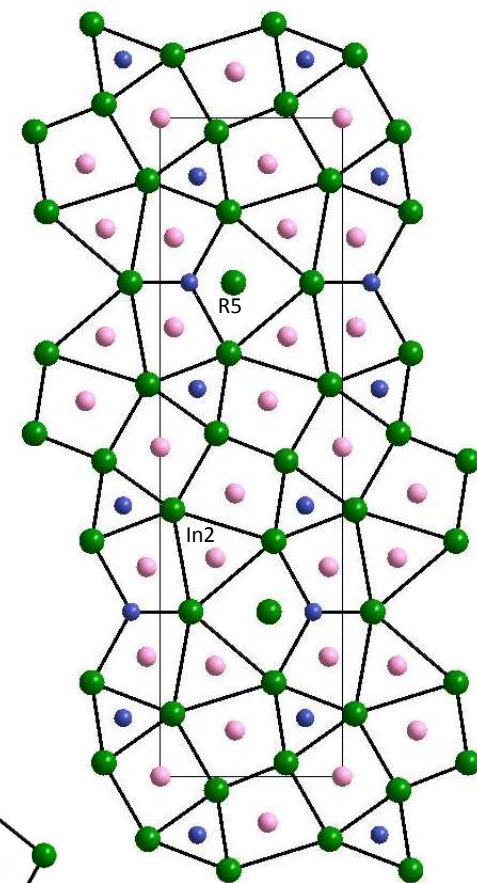
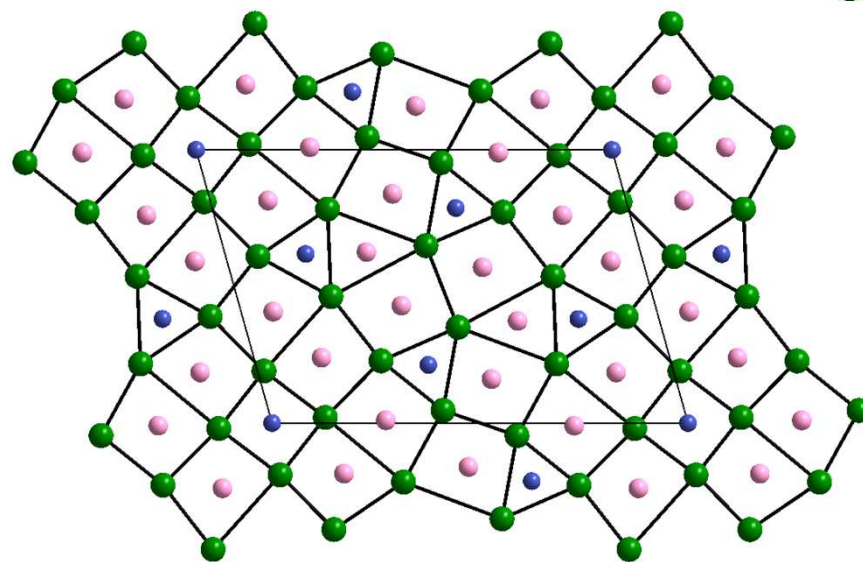
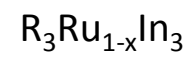
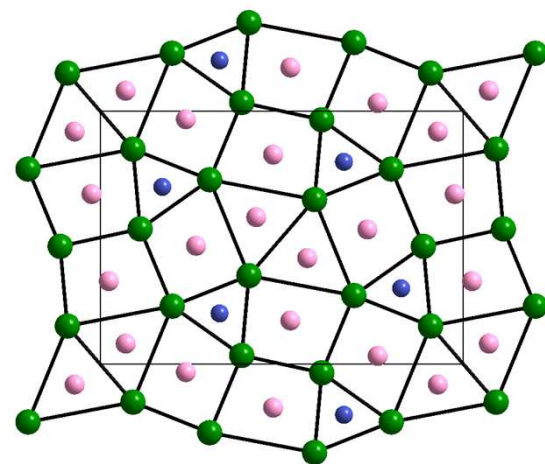
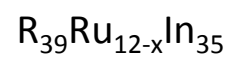
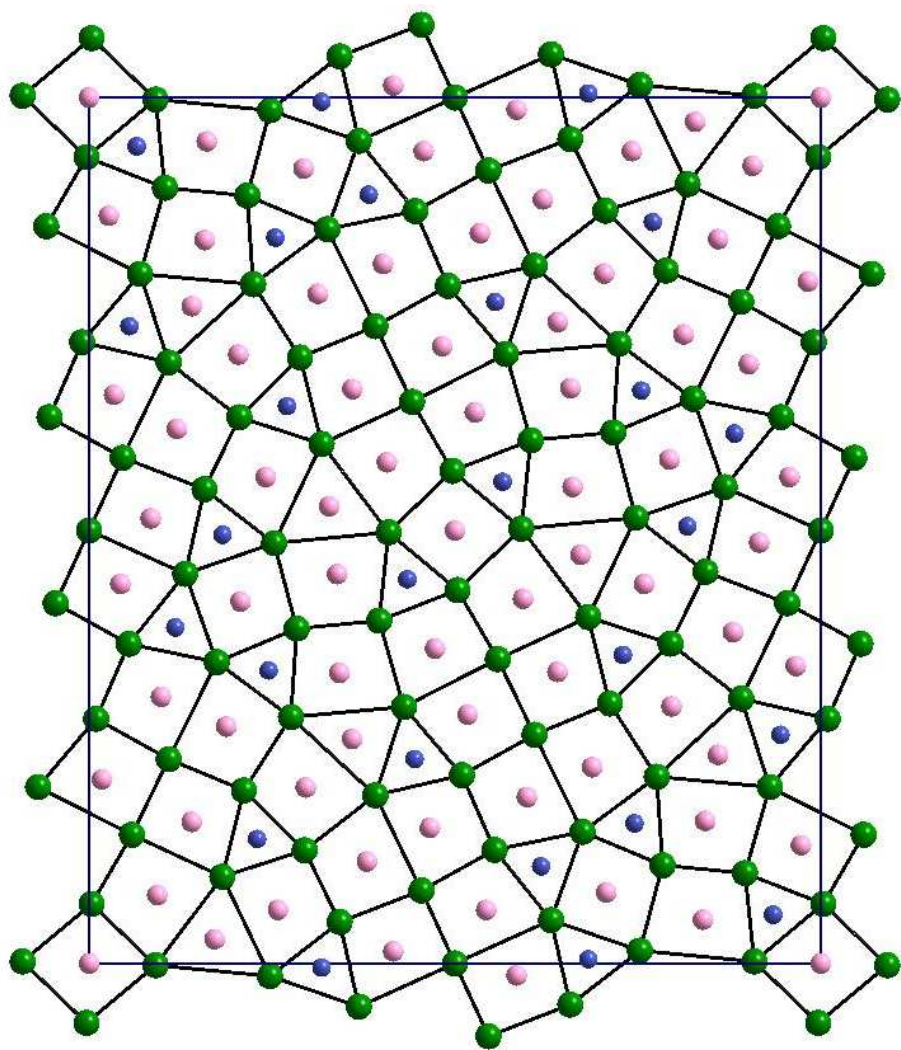
Empirical formula	Tb <sub>3</sub> Ru <sub>0.97</sub> In <sub>3</sub>	Ho <sub>3</sub> Ru <sub>0.96</sub> In <sub>3</sub>	Er <sub>3</sub> Ru <sub>0.91</sub> In <sub>3</sub>	Lu <sub>3</sub> Ru <sub>0.98</sub> In <sub>3</sub>	Ho <sub>16</sub> Ru <sub>5</sub> In <sub>14</sub>	Dy <sub>16</sub> Ru <sub>5</sub> In <sub>14</sub>
Structure type	Tb <sub>3</sub> Ru <sub>0.97</sub> In <sub>3</sub>	Tb <sub>3</sub> Ru <sub>0.97</sub> In <sub>3</sub>	Tb <sub>3</sub> Ru <sub>0.97</sub> In <sub>3</sub>	Tb <sub>3</sub> Ru <sub>0.97</sub> In <sub>3</sub>	Ho <sub>16</sub> Ru <sub>5</sub> In <sub>14</sub>	Ho <sub>16</sub> Ru <sub>5</sub> In <sub>14</sub>
Space group	<i>Pbam</i>	<i>Pbam</i>	<i>Pbam</i>	<i>Pbam</i>	<i>P2/m</i>	<i>P2/m</i>
Pearson symbol	<i>oP28</i>	<i>oP28</i>	<i>oP28</i>	<i>oP28</i>	<i>mP35</i>	<i>mP35</i>
Cell dimensions						
<i>a</i> , Å	11.338(7)	11.299(3)	11.289(8)	11.2601(3)	12.9267(6)	12.902(5)
<i>b</i> , Å	16.262(9)	16.195(3)	16.173(12)	16.0996(5)	3.5688(2)	3.5571(18)
<i>c</i> , Å	3.645(2)	3.6034(13)	3.590(6)	3.53820(10)	18.9908(9)	18.959(8)
$\beta$ , °					105.58(3)	105.58(4)
<i>V</i> , Å <sup>3</sup>	672.1(7)	659.4(3)	655.5(13)	641.42(3)	843.91(7)	838.1(6)
Calculated density, g cm <sup>-3</sup>	9.083	9.431	9.513	10.028	9.350	9.337
Radiation/ $\lambda$ , Å	Ag K $\alpha$ / 0.56087	Ag K $\alpha$ / 0.56087	Ag K $\alpha$ / 0.56087	Mo K $\alpha$ / 0.71073	Mo K $\alpha$ / 0.71073	Ag K $\alpha$ / 0.56087
Absorption coefficient, mm <sup>-1</sup>	22.961	25.450	26.831	58.407	48.467	24.910
Theta range	1.73÷19.96	1.73÷19.95	1.74÷21.96	3.11÷33.27	2.910÷27.485	0.88÷19.97
Range in <i>h</i> , <i>k</i> , <i>l</i>	0≤ <i>h</i> ≤13 -19≤ <i>k</i> ≤0 0≤ <i>l</i> ≤4	-13≤ <i>h</i> ≤0 -19≤ <i>k</i> ≤0 -4≤ <i>l</i> ≤3	-15≤ <i>h</i> ≤10 0≤ <i>k</i> ≤21 0≤ <i>l</i> ≤4	-18≤ <i>h</i> ≤18 -25≤ <i>k</i> ≤25 -3≤ <i>l</i> ≤5	-16≤ <i>h</i> ≤16 -4≤ <i>k</i> ≤4 -24≤ <i>l</i> ≤24	-15≤ <i>h</i> ≤15 0≤ <i>k</i> ≤4 0≤ <i>l</i> ≤23
Data/parameters	502/45	490/44	539/44	1306/45	1610/107	984/107
Goof on F <sup>2</sup>	0.976	0.983	0.981	1.06	1.167	0.943
R indices ( <i>I</i> >2 $\sigma$ <i>I</i> )	0.0346/ 0.0711	0.0376/ 0.0787	0.0517/ 0.1003	0.0305/ 0.0582	0.0553/ 0.0941	0.0633/ 0.1500
Extinction coefficient	0.00086(11)	-	-	0.00034(5)	-	-

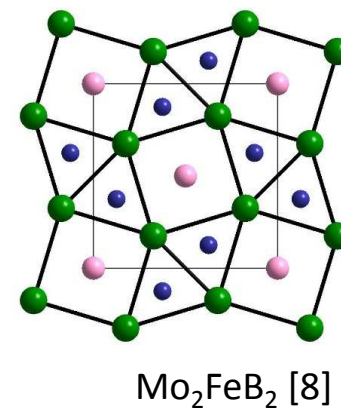
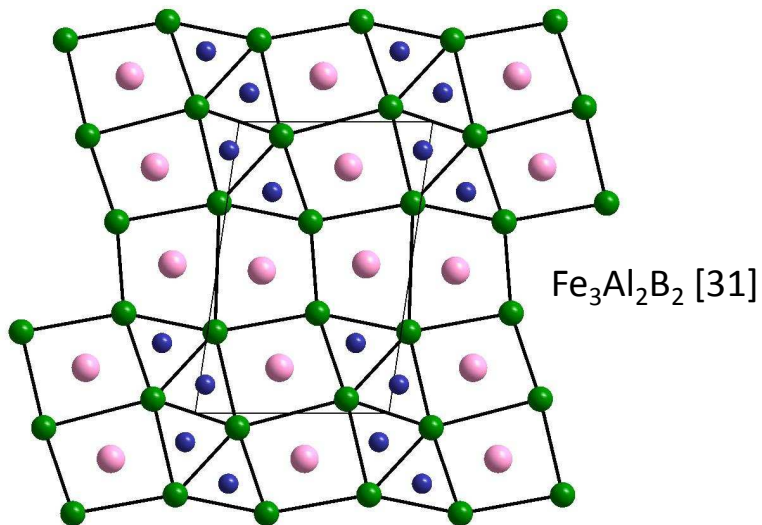
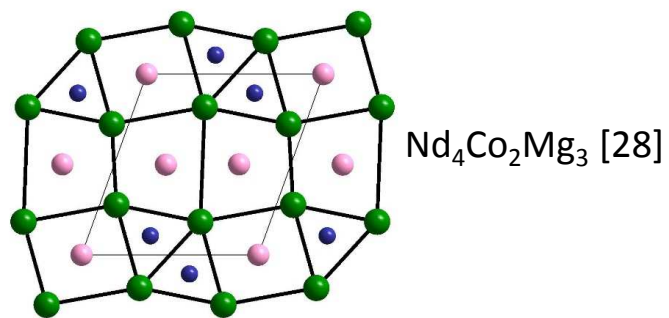
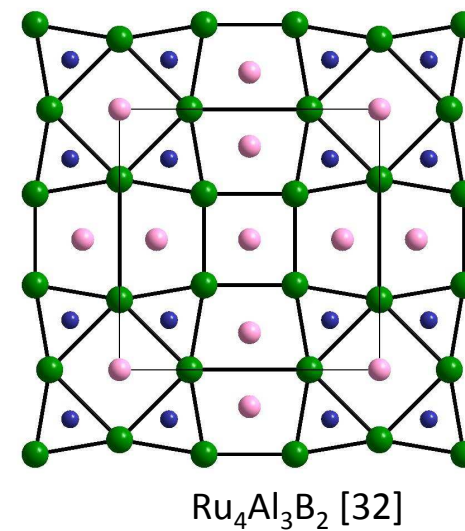
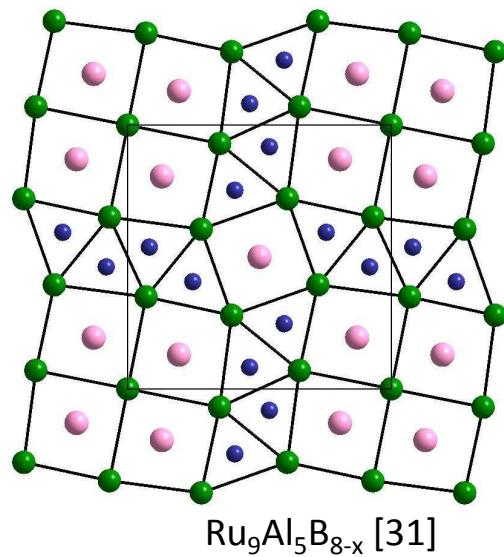
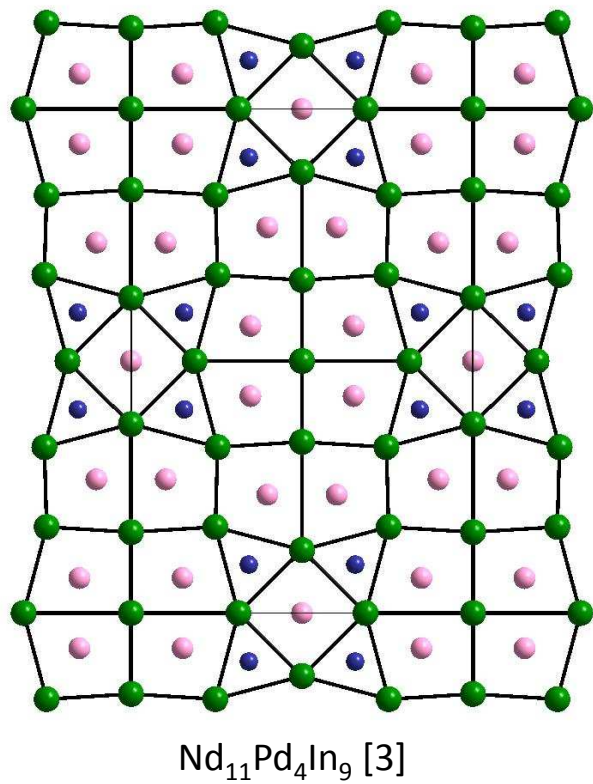
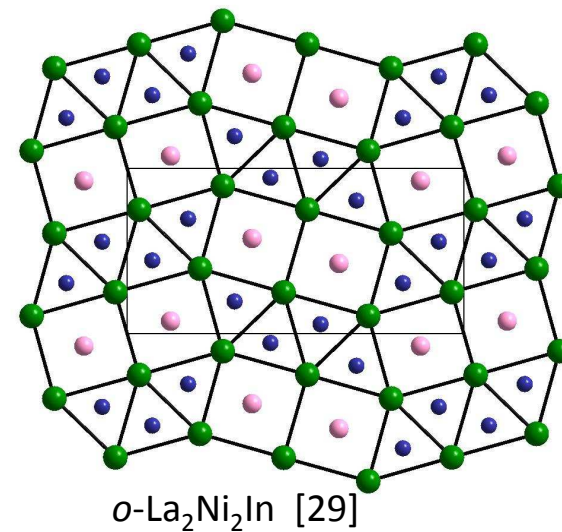
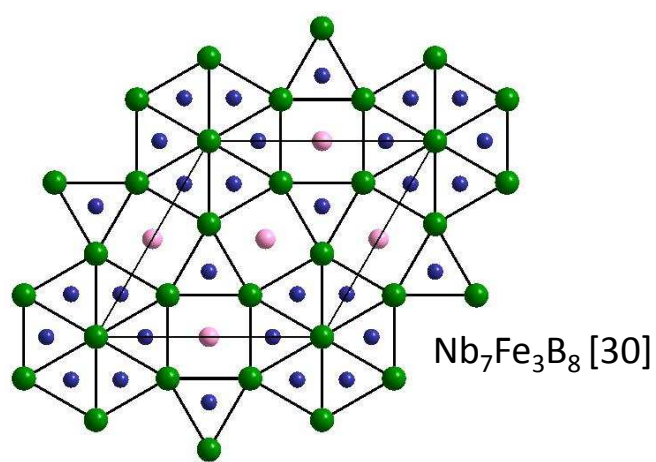
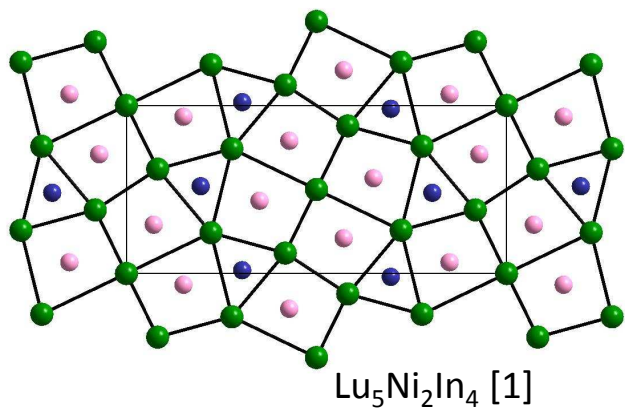
Table 1. Continued.

Empirical formula	Sm <sub>39</sub> Ru <sub>11.68</sub> In <sub>35</sub>	Gd <sub>39</sub> Ru <sub>11.63</sub> In <sub>35</sub>	Pr <sub>8</sub> Ru <sub>3</sub> In <sub>7</sub>	Sm <sub>7.72</sub> Ru <sub>3</sub> In <sub>7.28</sub>	Gd <sub>8</sub> Ru <sub>3</sub> In <sub>7</sub>	Tb <sub>7.60</sub> Ru <sub>3</sub> In <sub>7.40</sub>
Structure type	Nd <sub>39</sub> Ir <sub>10.98</sub> In <sub>36.02</sub>	Nd <sub>39</sub> Ir <sub>10.98</sub> In <sub>36.02</sub>	Y <sub>5</sub> Cu <sub>5</sub> Mg <sub>8</sub>	Y <sub>5</sub> Cu <sub>5</sub> Mg <sub>8</sub>	Y <sub>5</sub> Cu <sub>5</sub> Mg <sub>8</sub>	Y <sub>5</sub> Cu <sub>5</sub> Mg <sub>8</sub>
Space group	<i>Pbam</i>	<i>Pbam</i>	<i>Pmma</i>	<i>Pmma</i>	<i>Pmma</i>	<i>Pmma</i>
Pearson symbol	<i>oP172</i>	<i>oP172</i>	<i>oP36</i>	<i>oP36</i>	<i>oP36</i>	<i>oP36</i>
Cell dimensions						
<i>a</i> , Å	31.451(3)	31.366(10)	29.3940(13)	29.1608(17)	28.869(12)	28.7450(12)
<i>b</i> , Å	37.221(2)	37.09(3)	3.9128(2)	3.8509(2)	3.7660(12)	3.7364(2)
<i>c</i> , Å	3.7268(3)	3.6797(14)	8.1356(4)	8.1022(4)	8.030(3)	8.0883(3)
$\beta$ , °						
<i>V</i> , Å <sup>3</sup>	4362.8(6)	4281(4)	935.70(8)	909.84(8)	873.0(6)	868.71(7)
Calculated density, g cm <sup>-3</sup>	8.422	8.787	7.930	8.395	8.997	9.025
Radiation/ $\lambda$ , Å	Mo K $\alpha$ / 0.71073	Ag K $\alpha$ / 0.56087	Mo K $\alpha$ / 0.71073			
Absorption coefficient, mm <sup>-1</sup>	36.728	40.883	31.106	35.847	22.063	42.551
Theta range	2.910÷27.485	2.910÷27.485	1.386÷40.248	1.397÷45.091	1.11÷19.99	1.417÷45.199
Range in <i>h</i> , <i>k</i> , <i>l</i>	-39≤ <i>h</i> ≤40 -43≤ <i>k</i> ≤48 -4≤ <i>l</i> ≤4	-40≤ <i>h</i> ≤28 -48≤ <i>k</i> ≤47 -4≤ <i>l</i> ≤4	-39≤ <i>h</i> ≤53 -3≤ <i>k</i> ≤7 -14≤ <i>l</i> ≤14	-57≤ <i>h</i> ≤56 -4≤ <i>k</i> ≤7 -15≤ <i>l</i> ≤16	0≤ <i>h</i> ≤35 -2≤ <i>k</i> ≤4 0≤ <i>l</i> ≤9	-57≤ <i>h</i> ≤57 -7≤ <i>k</i> ≤7 -16≤ <i>l</i> ≤16
Data/parameters	3603/263	3760/263	2508/60	2713/64	605/59	2889/65
Goof on F <sup>2</sup>	1.150	1.062	1.036	1.037	1.080	1.017
R indices ( <i>I</i> >2 $\sigma$ <i>I</i> )	0.0494/0.0927	0.0653/0.1417	0.0380/0.0614	0.0625/0.1157	0.0538/ 0.1354	0.0524/0.1307
Extinction coefficient	-	-	0.00023(3)	0.00040(6)	-	0.00127(16)









16 new rare-earth ruthenium indides synthesized by a two-step reaction.

Crystal structures were studied by single-crystal and powder XRD.

The compounds are built of two layers stacking along the shortest axis.

Four new types of structure are described.

ACCEPTED MANUSCRIPT